Available online at www.sciencedirect.com
SCIENCE DIRECT®
Journal of Power Sources 146 (2005) 33–38
JOURNAL OF POWER SOURCES
www.elsevier.com/locate/jpowsour

The development of low cost $LiFePO_4$-based high power lithium-ion batteries

Kathryn Striebel *, Joongpyo Shim [1], Azucena Sierra, Hui Yang, Xiangyun Song, Robert Kostecki, Kathryn McCarthy

Environmental Energy Technologies Division, Lawrence Berkeley National Laboratory, Berkeley, CA 94720, USA

Available online 3 June 2005

Abstract

Pouch type $LiFePO_4$-natural graphite lithium-ion cells were cycled at constant current with periodic pulse-power testing in several different configurations. Components were analyzed after cycling with electrochemical, Raman and TEM techniques to determine capacity fade mechanisms. The cells with carbon-coated current collectors in the cathode and LiBOB-salt electrolyte showed the best performance stability. In many cases, iron species were detected on the anodes removed from cells with both TEM and Raman spectroscopy. The $LiFePO_4$ electrodes showed unchanged capacity suggesting that the iron is migrating in small quantities and is acting as a catalyst to destabilize the anode SEI in these cells.

Keywords: Lithium-ion; Post-test; $LiFePO_4$; LiBOB; Raman spectroscopy

1. Introduction

Much research has been devoted to the study of rechargeable lithium batteries for application in hybrid electric vehicles (HEVs), where low price, long calendar life, safety and high power capability are required [1,2]. The active materials found in consumer-size lithium batteries, such as the synthetic graphite MCMB and $LiCoO_2$, will need to be replaced with lower cost materials such as natural graphite and cathode materials, such as those containing iron and manganese.

In our previous studies of the $LiFePO_4$/natural graphite cell with a liquid electrolyte, we reported a limited cycle life for this cell system due to the consumption of the cycleable lithium at the anode by side reaction [3]. This was determined from post-test electrochemical analysis of the electrodes removed from the cycled cells [4]. The addition of a carbon coating to the Al current collector was found to improve the area specific impedance (ASI) of our pouch cells by as much as an order of magnitude. The improved cells also showed a 250% increase in cell cycle life for 100% DOD cycling at C/2, bringing this technology into the realm of possibility for applications requiring high power as well as high-energy. However, the capacity fade for these cells was still too high. Half-cell electrochemical diagnostics revealed that the electrodes maintained their original impedance and capacity, but that capacity was still fading due to the consumption of cycleable Li from the cell [5].

Many different mechanisms have been invoked for the explanation of capacity fade occurring in lithium-ion cells, most concerning the stability of one or both of the electrodes. Our laboratory has employed many techniques to examine various mechanisms for power and capacity fade observed in high power lithium-ion cells containing Co-doped $LiNiO_2$ and graphite, such as (1) degradation of active material, (2) impedance rise of cell by formation of SEI layer, (3) lithium inventory loss by side reaction and (4) loss of carbon as conductive additive from cathode, etc. [6–10]. In our previous work with the $LiNi_{0.8}Co_{0.15}Al_{0.05}O_2$ cells, performance loss was found to be a combination of loss of lithium inventory and structural degradation of the cathode active material and

* Corresponding author. Tel.: +1 510 486 4355; fax: +1 510 486 7303.
E-mail address: kastriebel@lbl.gov (K. Striebel).
[1] Present address: Kunsan National University, 68 Miryong-dong, Kunsan, Chonbuk 573-701, Republic of Korea.

0378-7753/$ – see front matter © 2005 Elsevier B.V. All rights reserved.
doi:10.1016/j.jpowsour.2005.03.119

impedance characteristics. In contrast, our early studies of $LiFePO_4$/natural graphite cells showed that lithium inventory loss and structural degradation of the anode were most important. The $LiFePO_4$ cathode appears to be exceptionally stable to long-term cycling [3,11].

In this paper, the performance of our $LiFePO_4$/natural graphite (NG) cell with different anodes is summarized and additional post-test analysis of selected components with Raman spectroscopy and TEM is presented. Early results showed that iron was detectable on the anodes removed from these cells. If the iron destabilizes the SEI layer on the graphite anode, in a similar fashion to that observed with Mn in the $Li_{1+y}Mn_{2-y}O_4$/graphite cell [12], removal of the HF source, and thereby the source of the iron dissolution from the system would be expected to alleviate this capacity fade mechanism. We, therefore, also report some preliminary results from $LiFePO_4$/NG cells without $LiPF_6$ in the electrolyte.

2. Experimental

The 12 cm^2 pouch cells contained $LiFePO_4$ cathodes and natural graphite anodes. Some of the electrodes were used as received from Hydro Quebec. Others were prepared in-house. All of the cathodes contained 82% carbon-coated $LiFePO_4$ (<1% carbon) from the University of Montreal, 8% conducting carbon and 10% PVdF binder (Kureha). The NMP slurries were cast onto three different types of current collector: (1) bare aluminum, (2) carbon-coated Al (C/Al) prepared in-house from a casting of 70 or 90% Shawinigan black in PVdF and (3) a commercially prepared collector prepared with a proprietary technique, courtesy of Hydro Quebec. The anodes were prepared from SL20 natural graphite (Superior Graphite), Hitachi Mag-10 graphite or SNG20, a spherical natural graphite (Hydro Quebec). They all contained 10% PVdF binder (Kureha) and copper current collectors.

The 10 mAh pouch cells were assembled with Celgard 2500 and filled with electrolyte in an Ar-filled glove-box. The cells were filled with either 1 M $LiPF_6$ + EC/DEC (1:1) (EM Science) or 0.7 M LiBOB salt in EC/DEC (1:1), courtesy of Ferro Chemical Corp. All cells were formed with two cycles at C/25. Cycle-life testing was carried out at constant (C/2) between 2.5 and 4.0 V. A reference performance test (RPT) with high-current discharge and charge pulses was carried out every 80 cycles to characterize the cell impedance and monitor the stability of this impedance during cycling or aging. More details of the manufacturing process and test protocol were described in previous work [5]. After cycling, several of the pouch cells were disassembled in the discharged state and each electrode was washed in DEC in the glove-box. Electrochemical, Raman and TEM post-test analysis was carried out on selected components.

The electrochemical analysis of electrodes before and after cycling was carried out in half-cells with Li reference and counter electrodes and the same electrolyte. An integrated confocal Raman microscope system "Labram" made by ISA Groupe Horiba was used to analyze and map the anode surface structure and composition. The excitation source was an internal He–Ne (632 nm) 10 mW laser. To avoid local overheating at the sample, the power of the laser beam was adjusted to 0.1 mW with neutral filters of various optical densities. The size of the laser beam at the sample was ~1.2 μm, which is about one order of magnitude smaller than the size of an average graphite particle. The average acquisition time for each spectrum was 40 s. The spectra were processed and deconvoluted using PeakFit 4.0 commercial software package. For TEM measurements, a part of the anode was dispersed in EMC, ground lightly and then some of the particles were collected on a copper grid. Sample preparation was carried out in the inert-atmosphere glove-box and the sample was then sealed in a small bottle for transportation to the Philips CM200/FEG (field emission gun) TEM at the National Center for Electron Microscopy (NCEM) at LBNL.

3. Results and discussion

The importance of carbon to the cycling of $LiFePO_4$ is well documented. The $LiFePO_4$ used in this work was prepared as a carbon-coated material from PhosTech. One might expect that no additional carbon, either in the cathode or on the current collector, would be required for good performance. However, our original cells with $LiFePO_4$ prepared on bare Al current collector showed unacceptably high ohmic losses [3]. Taking the lead from Hydro Quebec, $LiFePO_4$ cathodes were prepared on several different carbon-coated Al (C/Al) current collectors. The carbon coatings were less than 10 μm thick with <0.1 mg cm^2. The variable-rate discharge performance of $LiFePO_4$ cathodes prepared on a C/Al and a bare Al current collectors are compared in Fig. 1. The $LiFePO_4$ cathode on Al foil (left figure) shows large ohmic drops at high rates in the region of the flat plateau and a large decrease of specific capacity as rate is increased. The very thin carbon layer on the current collector (C/Al) appears to greatly reduce the contact resistance between electrode layer and current collector. The ohmic resistance of these cathodes, calculated from relaxation voltage at the end of discharge, decreased from about 200 to ~40 Ω cm^2 with addition of the coating on the current collector. Performance data from cells with four types of current collector are shown in Fig. 2. Based on these results, the remainder of the cells discussed in this paper comprised cathodes cast onto either the HQ CC or the LBNL–C/Al CC with 90% carbon black in the coating.

The cycle performance of $LiFePO_4$/natural graphite pouch cells prepared from either the LBNL–C/Al or the HQ current collectors are compared in Fig. 3. It should be noted that there are three different graphite anodes used in these cells. Both cyclability and coulombic efficiency (not shown) are significantly improved with the use of the C/Al in the cathode. Part of the improvement can be traced directly to the lower impedance of the cells with the C/Al. The two cells with

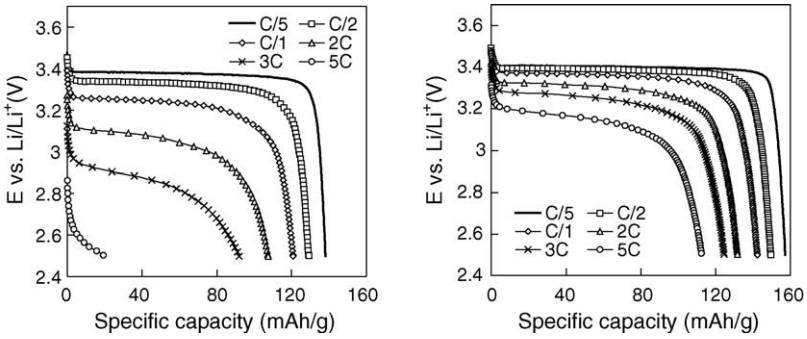

Fig. 1. Discharging voltage profiles of $LiFePO_4$ cathodes on only Al foil (left) and carbon-coated Al foil (right) for various C rates. Charging rate C/2.

the SNG20 anode show an improvement in capacity stability on switching from $LiPF_6$ to LiBOB-containing electrolyte. In fact, the initial rate of capacity fade in the LiBOB cell was half that of the $LiPF_6$ cell. This improvement in stability was even more dramatic at elevated temperatures (not shown). Fig. 4 shows the area specific impedance (ASI), calculated from a reference performance test [13], of these pouch cells before cycling, unless noted. The ASI of cell with the LBNL–C/Al in the $LiFePO_4$ cathode is significantly lower than the cell with $LiFePO_4$ cathode on uncoated Al, but more significantly, this low impedance is maintained during cycling. The initial ASI from the cell with HQ components was intermediate to the other two. The ASI of the LBNL–C/Al cell after 400 cycles is much lower than that of older cells after 80 cycles. However, the improved cell still has a high capacity fade rate of about 0.1% cycle. Our target for these pouch cells is 0.05% cycle or a loss of 20% of the C/2 capacity loss after 400 cycles. Very little difference was observed in the initial impedance of the cells with $LiPF_6$ versus LiBOB electrolytes. This suggests that in this cell with a relatively low conductivity cathode that the ionic conductance of the electrolyte is not a rate-limiting factor.

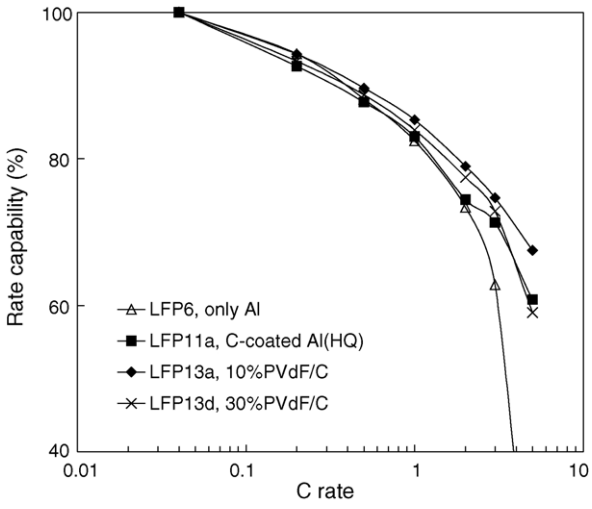

Fig. 2. Peukert plots for half-cell studies of the variable rate discharge for $LiFePO_4$ cathodes prepared on four types of current collectors.

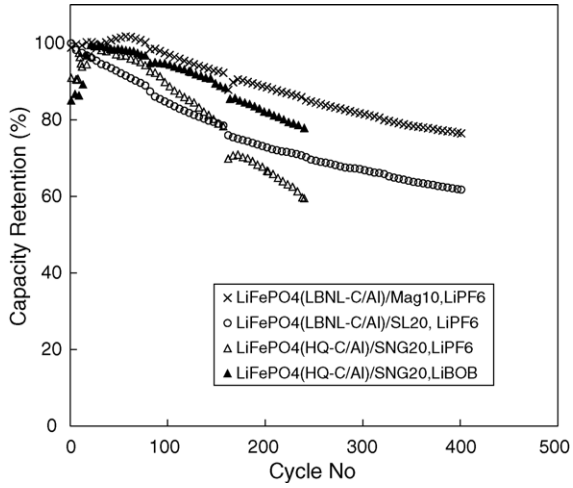

Fig. 3. Cycle performance for $LiFePO_4$ cells with Mag-10, SL20 and SNG20(HQ) anodes in either $LiPF_6$ or LiBOB electrolyte, constant current C/2 cycling, 25 °C.

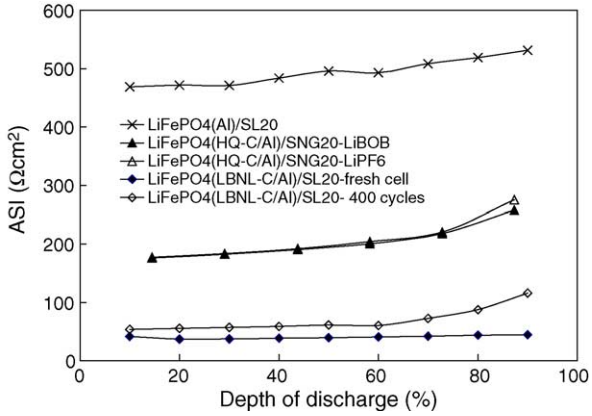

Fig. 4. Area specific impedance (ASI) of pouch cells calculated from the reference performance test (18 s discharge pulse).

To understand more about the fade mechanisms operative in these cells, several of the cells were fully discharged at C/25 before disassembly in the glovebox for post-test diagnostic analysis. The consumption of cycleable Li from the cell is demonstrated in Fig. 5. The first charge of the cycled cathode, in a half-cell against lithium, reveals how much cycleable lithium remains in the cell after cycling. The anode samples showed voltages greater than 1.5 V versus Li

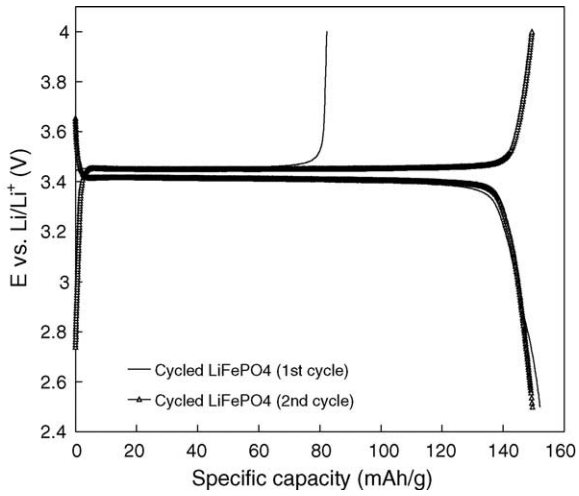

Fig. 5. Voltage profile of cycled cathode at C/25 in half-cell against fresh Li metal.

indicating that there is no cycleable Li remaining. Comparison of this first charge capacity with the full capacity on the second cycle shows that the cycled $LiFePO_4$ cathode contains only 55% of the original Li content after formation and cycling. About 24% was lost during anode formation and the balance of about 21% was lost during cycling. Comparison with the fresh cathode capacity shows that the performance of the cycled cathode has not deteriorated; only the inventory of the lithium is lost. This loss is usually associated with the continual formation of the SEI, possibly accompanied by the dissolution of the SEI. We observed gassing in these pouch cells during cycling, consistent with a continual oxidation of the electrolyte solvent(s). The performance of the anodes removed from these cells was similar to that of fresh anodes [5]. This suggests that during this side-reaction, the SEI is maintaining steady thickness, or at least a high conductivity. Several side-reactions with the electrolyte have been proposed. For the $Li_{1+y}Mn_{2-y}O_4$/graphite cell, a mechanism for the destabilization of the SEI on the anode has been proposed involving deposition of manganese, liberated form the $Li_{1+y}Mn_{2-y}O_4$ cathode by proton attack [12]. The source of protons is the well-known degradation of the $LiPF_6$ by reaction with residual water. The improvement in cycling stability of the $LiFePO_4$ cells with a non-$LiPF_6$-containing electrolyte, suggests a similar mechanism. However, in the case of the spinel cathode, the cathode itself has been found to loose capacity though the loss of Mn, whereas in these cells, the $LiFePO_4$ cathode capacity is stable [5]. However, the destabilization of the anode-SEI could be due to the catalytic effect of small amounts of iron impurities, dissolved from the surface or bulk of the $LiFePO_4$, in quantities undetectable by XRD.

3.1. Raman analysis of the anodes

Anodes removed from these cells were analyzed with micro-Raman high-resolution mapping. Raman spectroscopy

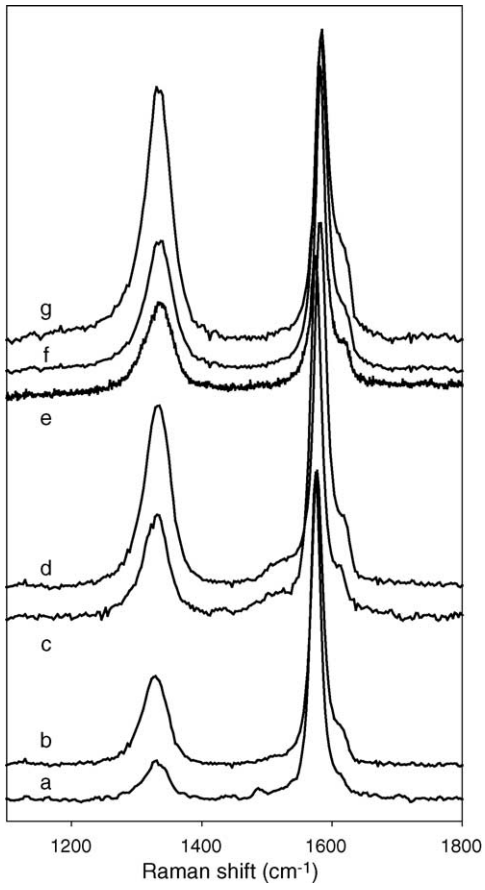

Fig. 6. Average Raman spectra of graphite anodes: Mag-10 fresh anode (a), Mag-10 cycled in LiPF6 electrolyte (b), SL20 fresh anode (c), SL20 cycled in LiPF6 electrolyte (d), SNG20 fresh anode (e), SNG20 cycled in LiPF6 electrolyte (f) and SNG20 cycled in LiBOB electrolyte (g).

is useful for characterizing the near-surface structure of graphite because of its relatively large Raman scattering cross-section. A typical Raman spectrum of graphite consists of two peaks: a strong (G) band at ~1583 cm^{-1} and (D) band at 1345 cm^{-1}, which is associated with the breakage of symmetry occurring at the edges of the graphite sheets. The relative intensity of the D band versus G band is attributed to the level of carbon disorder in microcrystalline graphite [14] and is inversely proportional to the intra-planar microcrystallite distance L_a [15].

Average Raman spectra from representative 52 μm × 75 μm areas of a fresh graphite anode and the cycled anodes are presented in Fig. 6. Two sharp carbon bands are always present at ~1345 and ~1583 cm^{-1}. However, the relative D and G peak intensities change significantly for the cycled anodes. The D band intensity increases substantially whereas the G band broadens noticeably. The D/G band ratio for fresh and cycled anodes calculated from the deconvoluted Raman spectra of the three different types of graphite are listed in Table 1. This ratio always increased with cycling for all of the tested anodes, compared with the fresh electrodes. However, the anodes cycled in the LiBOB electrolytes display less disordered carbon on the surface at the end of testing than

Table 1
D/G ratios for analyzed anodes after cycling against $LiFePO_4$ cathodes

D/G	Mag-10 ($LiPF_6$)	SL20 ($LiPF_6$)	SNG20 ($LiPF_6$)	SNG20 (LiBOB)
Fresh anode	0.25	0.4	0.62	0.62
Cycled anode	0.52	0.8	1.14	0.86
Number of cycles	400	400	240	240
Percent change	+108	+100	+84	+39

the anodes removed from cells with the $LiPF_6$-containing electrolyte.

Some of the observed carbon disordering might be inherent to the formation process. However, earlier studies Li-ion cells with Mag-10 graphite showed that the formation process does not lead to an increase in anode disorder but that this ratio increases with the extent of cycling [10,16]. We found only a moderate (24%) increase in the D/G band ratio for a Mag-10 anode that was cycled 480 times against a $LiNi_{0.8}Co_{0.15}Al_{0.05}O_2$ cathode at room temperature, which also showed very little loss of performance.

The presence of disordered carbonaceous material in the anode may be explained by local graphite degradation/exfoliation by the co-intercalation of ion aggregates and protons [17], localized high rate of lithium intercalation [8], or carbon black additive migration from the composite cathode to the anode. In all instances, graphite structure breakdown and/or deposition of carbon black will lead to the exposure of new graphene edges and fragments of graphene planes to the electrolyte. These freshly exposed active carbon sites react readily with the electrolyte to form inorganic products such as phosphates, carbonates and LiF. This process results the long-term accumulation of inorganic products at the anode as well as the transfer of cycleable lithium from the cathode to the anode SEI, which limits the Li-ion cell capacity.

A semi-quantitative Raman microscopy analysis of the anode surface was carried out by high-resolution Raman surface composition mapping. Thousands of Raman spectra were collected systematically from 52 μm × 75 μm sections of anode surfaces at 0.7 μm resolution, and then deconvoluted, and

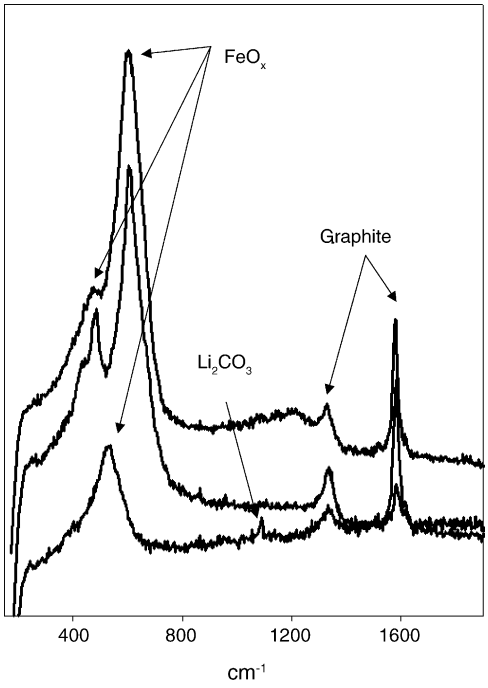

Fig. 7. Raman microscope spectra recorded form different locations on the surface of anodes from cells cycled in LiPF6-containing electrolyte.

analyzed. In marked contrast to graphite D and G bands at 1345 and 1583 cm^{-1}, respectively, Raman spectra collected at a few locations on the anode surface displayed a group of bands at 418, 480, 530 and 605 cm^{-1} and a weak shoulder at ca. 650 cm^{-1} (Fig. 7). Similar Raman spectra have been reported for α-Fe_2O_3 and Fe_3O_4 but the observed Raman frequencies and peak relative intensities are slightly different from literature values [18,19]. Since formation conditions for iron oxides can strongly affect the resulting degree of crystallinity, defect- or impurity-induced lattice modification or the presence of multiple phases, one could reasonably expect differences in the Raman spectra of iron FeO_x species of nominally identical chemical composition. Interestingly, we detected iron oxide impurities on the surface of anodes that were cycled in $LiPF_6$-containing electrolytes. There was

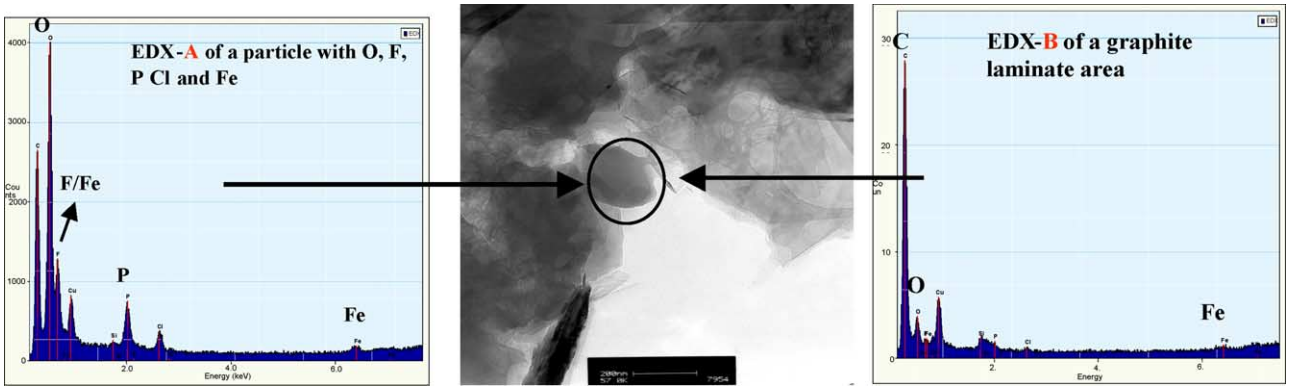

Fig. 8. TEM analysis of an SL-20 anode after cycling with a $LiFePO_4$ cathode: (A) EDX of a particle on the anode sample showing the Fe-containing "impurity" after cycling, (B) TEM image, 57,000× and (C) EDX from "bulk" portion of the anode sample.

no clear indication of iron oxide deposition on the surface of graphite anodes that were tested in the LiBOB electrolyte. A small band at 1087 cm^{-1} corresponds to the carbonate group symmetric stretching vibration from Li_2CO_3 in the SEI layer.

3.2. TEM analysis of the anodes

Further confirmation of the presence of the iron on several anodes removed form $LiFePO_4$/$LiPF_6$/NG cells was obtained with TEM and electron diffraction analysis. Fig. 8B shows the TEM image with two areas analyzed with EDX (Fig. 8A and C). Fig. 8A shows a small amount of Fe present in the particle of the sample. Several similar particles were observed in the generally graphitic mass. The parallel measurement on anodes removed form the $LiFePO_4$/LiBOB/NG cells is the subject of future work.

4. Conclusions

The addition of a carbon-coated current collector to the cathode of the $LiFePO_4$/natural graphite cell lead to 2.5 times improvement in cyclability. In addition, the cell impedance was reduced by an order of magnitude and the impedance rise during cycling was only a few percent. Post-test analysis of cycled anodes with Raman spectroscopy showed evidence of iron species deposited on the anodes during cycling. The amount of iron was not significant enough to affect the capacity of the $LiFePO_4$ positive electrodes. However, it is possible that this iron acts to catalyze the instability of the anode and consume the cycleable Li from the cell. While the anode half-cell performance was not severely affected when matched against a Li metal foil, the effective increase in disorder of the graphite surface was four times that observed for a similar anode cycled against a $LiNiCoAlO_2$ cathode for the same number of cycles. The presence of iron was confirmed with TEM measurements and the pattern of deposition was similar to that observed in an anode cycled against a $Li_{1+y}Mn_{2-y}O_4$ cathode. It is believed that this iron may be etched from the surface for the $LiFePO_4$ particles in a mechanism involving HF, since preliminary results with non-HF containing electrolytes, i.e. LiBOB-salt electrolytes show better capacity retention and less direct evidence of Fe on the surface of the anodes. More work on this degradation mechanism is clearly warranted.

Acknowledgements

We gratefully acknowledge the supply of LiBOB electrolytes from Ferro Chemical Corp. and the supply of electrode materials from Hydro-Quebec, U. de Montreal and Superior Graphite. This work was supported by the Assistant Secretary for Energy Efficiency and Renewable Energy, Office of FreedomCAR and Vehicle Technologies of the U.S. Department of Energy under Contract No. DE-AC03-76SF00098.

References

[1] T.Q. Duong, J. Power Sources 89 (2000) 244.
[2] N. Terada, T. Yanagi, S. Arai, M. Yoshikawa, K. Ohta, N. Nakajima, N. Arai, J. Power Sources 100 (2001) 80.
[3] J. Shim, K.A. Striebel, J. Power Sources 119–121 (2003) 955.
[4] J. Shim, A. Sierra, K.A. Striebel, 202nd Meeting of the Electrochemistry Society, Salt Lake City, USA, October, 2002 (Abstract #123).
[5] J. Shim, A.E. Sierra, K.A. Striebel, The development of $LiFePO_4$-based high power lithium-ion batteries, in: A. Landgrebe (Ed.), Power Sources for Transportation Applications, PV 2003-24, Electrochemistry Society, Orlando, FL, Fall, 2003.
[6] X. Zhang, P.N. Ross, R. Kostecki, F. Kong, S. Sloop, J.B. Kerr, K.A. Striebel, E.J. Cairns, F. McLarnon, J. Electrochem. Soc. 148 (2001) A463.
[7] J. Shim, R. Kostecki, T. Richardson, X. Song, K.A. Striebel, J. Power Sources 112 (2002) 222.
[8] R. Kostecki, F. McLarnon, J. Power Sources 119–121 (2003) 550.
[9] R. Kostecki, F. McLarnon, Electrochem. Solid-State Lett. 5 (2002) A164.
[10] K.A. Striebel, J. Shim, E.J. Cairns, R. Kostecki, Y.-J. Lee, J. Reimer, T.J. Richardson, P.N. Ross, X. Song, G.V. Zhuang, J. Electrochem. Soc 151 (2004) A857.
[11] K.A. Striebel, A. Guerfi, J. Shim, M. Armand, M. Gauthier, K. Zaghib, J. Power Sources 119–121 (2003) 951.
[12] G. Amatucci, A. DuPasquier, A. Blyr, T. Zheng, J.M. Tarascon, Electrochim. Acta 45 (1999) 255.
[13] PNGV Battery Test Manual, INEEL, DOE/ID-10597, Rev. 3, 2001.
[14] R. Vidano, D.B. Fischbach, J. Am. Ceram. Soc. 61 (1978) 13.
[15] F. Tuinstra, J.L. Koenig, J. Chem. Phys. 53 (1976) 1126.
[16] FY 2002 Progress Report for Energy Storage Research and Development, which can be downloaded from the U.S. Department of Energy web site at http://www.eere.energy.gov/vehiclesandfuels/resources/fcvt_publications.shtml.
[17] E. Peled, D. Bar Tow, A. Merson, A. Gladkich, L. Burstein, D. Golodnitsky, J. Power Sources 97–98 (2001) 52.
[18] I.R. Beattie, T.R. Gilson, J. Chem. Soc. A 5 (1983) 980.
[19] D.L.A. de Faria, S. Venâncio Silva, M.T. de Oliveira, J. Raman Spectrosc. 28 (1997) 873.